Journal of Computational Physics 250 (2013) 106–125

Contents lists available at SciVerse ScienceDirect

Journal of Computational Physics

journal homepage: www.elsevier.com/locate/jcp

Weak Galerkin methods for second order elliptic interface problems

Lin Mu [a], Junping Wang [b,1], Guowei Wei [a,2], Xiu Ye [c,3], Shan Zhao [d,*,4]

[a] Department of Mathematics, Michigan State University, East Lansing, MI 48824, United States
[b] Division of Mathematical Sciences, National Science Foundation, Arlington, VA 22230, United States
[c] Department of Mathematics and Statistics, University of Arkansas at Little Rock,Little Rock, AR 72204, United States
[d] Department of Mathematics, University of Alabama, Tuscaloosa, AL 35487, United States

ARTICLE INFO

Article history:
Received 31 January 2012
Received in revised form 9 January 2013
Accepted 28 April 2013
Available online 23 May 2013

Keywords:
Finite element methods
Weak Galerkin method
Second order elliptic interface problems
Nonsmooth interface
Low solution regularity

ABSTRACT

Weak Galerkin methods refer to general finite element methods for partial differential equations (PDEs) in which differential operators are approximated by their weak forms as distributions. Such weak forms give rise to desirable flexibilities in enforcing boundary and interface conditions. A weak Galerkin finite element method (WG-FEM) is developed in this paper for solving elliptic PDEs with discontinuous coefficients and interfaces. Theoretically, it is proved that high order numerical schemes can be designed by using the WG-FEM with polynomials of high order on each element. Extensive numerical experiments have been carried out to validate the WG-FEM for solving second order elliptic interface problems. High order of convergence is numerically confirmed in both L_2 and L_∞ norms for the piecewise linear WG-FEM. Special attention is paid to solve many interface problems, in which the solution possesses a certain singularity due to the nonsmoothness of the interface. A challenge in research is to design nearly second order numerical methods that work well for problems with low regularity in the solution. The best known numerical scheme in the literature is of order $\mathcal{O}(h)$ to $\mathcal{O}(h^{1.5})$ for the solution itself in L_∞ norm. It is demonstrated that the WG-FEM of the lowest order, i.e., the piecewise constant WG-FEM, is capable of delivering numerical approximations that are of order $\mathcal{O}(h^{1.75})$ to $\mathcal{O}(h^2)$ in the L_∞ norm for C^1 or Lipschitz continuous interfaces associated with a C^1 or H^2 continuous solution.

1. Introduction

In this paper, we are concerned with interface problems for second order elliptic partial differential equations (PDEs) with discontinuous coefficients and singular sources. For simplicity, consider the model problem of seeking functions $u = u(x, y)$ and $v = v(x, y)$ satisfying

* Corresponding author. Tel.: +1 205 3485155.
E-mail addresses: linmu@mail.math.msu.edu (L. Mu), jwang@nsf.gov (J. Wang), wei@math.msu.edu (G. Wei), xxye@ualr.edu (X. Ye), szhao@bama.ua.edu (S. Zhao).

[1] The research of Wang was supported by the NSF IR/D program, while working at the Foundation. However, any opinion, finding, and conclusions or recommendations expressed in this material are those of the author and do not necessarily reflect the views of the National Science Foundation.
[2] This research of Wei was supported in part by National Science Foundation Grants CCF-0936830 and DMS-1160352, and NIH Grant R01GM-090208.
[3] This research of Ye was supported in part by National Science Foundation Grant DMS-1115097.
[4] The research of Zhao was supported in part by National Science Foundation Grant DMS-1016579.

0021-9991/$ - see front matter © 2013 Elsevier Inc. All rights reserved.
http://dx.doi.org/10.1016/j.jcp.2013.04.042

$$-\nabla \cdot A_1 \nabla u = f_1, \quad \text{in } \Omega_1, \tag{1.1}$$
$$-\nabla \cdot A_2 \nabla v = f_2, \quad \text{in } \Omega_2, \tag{1.2}$$
$$u = g_1, \quad \text{on } \partial\Omega_1 \setminus \Gamma, \tag{1.3}$$
$$v = g_2, \quad \text{on } \partial\Omega_2 \setminus \Gamma, \tag{1.4}$$
$$u - v = \phi, \quad \text{on } \Gamma, \tag{1.5}$$
$$A_1 \nabla u \cdot \mathbf{n}_1 + A_2 \nabla v \cdot \mathbf{n}_2 = \psi, \quad \text{on } \Gamma, \tag{1.6}$$

where $\Omega = \Omega_1 \cup \Omega_2$, $\Gamma = \Omega_1 \cap \Omega_2$, $\partial\Omega_1 \setminus \Gamma \neq \{\varnothing\}$ and $\mathbf{n}_1$ and $\mathbf{n}_2$ are outward normals of Ω_1 and Ω_2. Here, f_1 and f_2 can be singular and Γ may be of Lipschitz continuous. This problem is commonly referred to as an elliptic interface problem and occurs widely in practical applications, such as fluid mechanics [23], electromagnetic wave propagation [14,18,41,40], materials science [20,22], and biological science [39,12,7]. The finite difference based solution of elliptic interface problems was pioneered by Peskin with his immersed boundary method (IBM) in 1977 [30,29]. Mayo constructed an interesting integral equation approach to this class of problems [25]. To properly solve the elliptic interface problem, one needs to enforce additional interface conditions (1.5) and (1.6). LeVeque and Li advanced the subject with their second order sharp interface scheme, the immersed interface method (IIM) [24]. In the past decades, many other elegant methods have been proposed, including the ghost fluid method (GFM) proposed by Fedkiw, Osher and coworkers [11], finite-volume-based methods [28], the piecewise-polynomial discretization [8], and matched interface and boundary (MIB) methods [41,43,37].

A proof of second order convergence of the IIM for smooth interfaces was due to Beale and Layton [2]. Rigorous convergence analysis of most other finite difference based elliptic interface schemes is not available yet. In general, it is quite difficult to analyze the convergence of finite difference based interface schemes because conventional techniques used in Galerkin formulations are not applicable for collocation schemes. The analysis becomes particularly difficult when the designed elliptic interface scheme is capable of dealing with nonsmooth interfaces [37]. At present, there is no rigorous convergence analysis available for elliptic interface methods that delivery high-order accuracy for nonsmooth interfaces, to the authors' knowledge.

Finite element methods (FEMs) are another class of important approaches for elliptic interface problems. The construction of FEM solutions to elliptic interface problems dates back to 1970s [1], and has been a subject of intensive investigation in the past few decades [10,31,17,6]. Since the elliptic interface problem defined in Eqs. (1.1)–(1.6) provides opportunities to construct new FEM schemes, a wide variety of FEM approaches have been proposed in the literature. There are two major classes of FEM based interface methods, namely, interface-fitted FEMs and immersed FEMs, categorized according to the topological relation between discrete elements and the interface. In the interface-fitted FEMs, or body-fitted FEMs, the finite element mesh is designed to align with the interface. Local mesh refinement based a priori and/or posteriori error estimation can be carried out. The performance of interface-fitted FEMs depends on the quality of the element mesh near the interface as well as the formulation of the problem. In fact, the construction of high quality FEM meshes for real world complex interface geometries is an active area of research. Bramble and King discussed an FEM for nonhomogeneous second order elliptic interface problems on smooth domains [4]. One way to deal with embedded interface conditions is to use distributed Lagrange multipliers [5], In fact, similar ideas have been widely used in mortar methods and fictitious domain methods for the treatment of embedded boundaries [13]. A Q_1-nonconforming finite element method was also proposed for elliptic interface problems [31]. Discontinuous Galerkin (DG) FEMs have been developed for elliptic equations with discontinuous coefficients [9,17]. Inherited from the original DG method, DG based interface schemes have the flexibility to implement interface jump conditions.

Immersed FEMs are also effective approaches for embedded interface problems [10,35,15,21,16]. A key feature of these approaches is that their element meshes are independent of the interface geometry, i.e., the interface usually cuts through elements. As such, there is no need to use the unstructured mesh to fit the interface, and simple structured Cartesian meshes can be employed in immersed FEMs. Consequently, the time-consuming meshing process is bypassed in immersed FEMs. However, to deal with complex interface geometries, it is necessary to design appropriate interface algorithms, which are similar to finite-difference based elliptic interface methods. In fact, immersed FEMs can be regarded as the Galerkin formulations of finite difference based interface schemes. It is not surprised that key ideas of many immersed FEMs actually come from the corresponding finite-difference based interface schemes. Additionally, other ideas in numerical analysis have been utilized for the construction of immersed FEMs. For example, a stabilized Lagrange multiplier method based on Nitsche technique has been used to enforce interface jump constraints [16]. The performance of immersed FEMs depends on the design of elegant interface schemes for complex interface geometries.

Convergence analysis of FEM based elliptic interface methods has been considered by many researchers. Unlike the collocation formulation, the Galerkin framework of FEMs allows more rigorous and robust convergence analysis. Cai et al. gave a proof of convergence for a DG FEM for interface problems [6]. Dryja et al. discussed the convergence of the DG discretization of Dirichlet problems for second-order elliptic equations with discontinuous coefficients in 2D [9]. Hiptmair et al. presented a convergence analysis of $H(\text{div};\Omega)$-elliptic interface problems in general 3D Lipschitz domains with smooth material interfaces [19]. Recently, an edge-based anisotropic mesh refinement algorithm has been analyzed and applied to elliptic interface problems [33].

Despite of numerous advancements in the numerical solution of interface problems, there are still a few remaining challenges in the field. One of these challenges concerns the construction of higher order interface schemes. Currently, most interface schemes are designed to be of second order convergence. However, higher order methods are efficient and

desirable for problems associated with high frequency waves, such as electromagnetic and acoustic wave propagation and scattering, vibration analysis of engineering structures, and shock-vortex interaction in compressible fluid flows. It is easy to construct high order methods and even spectral methods for these problems with straight interfaces in simple domains. However, it is difficult to obtain high order convergence when the interface geometries are arbitrarily complex. A fourth order MIB scheme has been developed for the Helmholtz equation in media with arbitrarily curved interfaces in 2D [40]. Up to sixth order MIB schemes have been constructed for the Poisson equation with ellipsoidal interfaces in 3D [37]. There are two standing open problems concerning high order elliptic interface schemes, i.e., the construction of fourth-order 3D interface schemes for arbitrarily complex interfaces with sharp geometric singularities and the construction of sixth-order 3D interface schemes for arbitrarily curved smooth interfaces [37].

Another challenging issue in elliptic interface problems arises from nonsmooth interfaces or interfaces with Lipschitz continuity [39,38,36,21]. Nonsmooth interfaces are also referred to as geometric singularities, such as sharp edges, cusps and tips, which commonly occur in real-world applications. It is a challenge to design high order interface schemes for geometric singularities both numerically and analytically. The first known second order accurate scheme for nonsmooth interfaces was constructed in 2007 [38]. Since then, many other interesting second order schemes have been constructed for this class of problems in 2D [8,21,3] and 3D [37]. The second order MIB method for 3D elliptic PDEs with arbitrarily non-smooth interfaces or geometric singularities has found its success in protein electrostatic analysis [39,12,7]. However, it appears truly challenging to develop fourth order schemes for arbitrarily shaped nonsmooth interfaces in 3D domains, although fourth order schemes have been reported for a few special interface geometries [37]. Due to the need in practical applications, further effort in this direction is expected.

The above mentioned difficulties in the solution of interface problems with geometric singularities significantly deteriorate in certain physical situations. It is well-known that the electric field diverges near the geometric singularities, such as tips of electrodes, antenna and elliptic cones, and sharp edges of planar conductors. Since electric field is related to the gradient of the electrostatic potential, i.e., the solution of the Poisson equation in the electrostatic analysis, it turns out that the solution of the elliptic equation has a lower regularity, e.g., the gradient does not exist at the geometric singularities. For isolated singularities, one can alleviate the difficulty by introducing an algebraic factor to solve a regularized equation whose solution has a high regularity [39,36]. In this manner, second order MIB schemes have been constructed in the past [39,36]. However, it is also desirable to directly solve the original PDEs with a low solution regularity. The FEM developed by Hou et al. is of 1.5th order convergence in the solution and 0.65th order convergence in the gradient of the solution when the solution of the Poisson equation is H^2 continuous and the interface is C^1 or Lipschitz continuous [21]. If the solution is only C^1 continuous, the convergence orders of the solution and the gradient become 1 and 0.75, respectively [21]. In fact, due to the low solution regularity induced by the nonsmooth interface, it is very difficult to analyze the convergence of numerical schemes because commonly used techniques may no longer be available. Therefore, there is a pressing need to develop both high order numerical methods and rigorous analysis of numerical methods for elliptic interface problems with low solution regularities induced by geometric singularities.

The objective of the present work is to construct a new numerical method for elliptic equations with low solution regularities induced by nonsmooth interfaces. To this end, we employ a newly developed weak Galerkin finite element method (WG-FEM) by Wang and Ye [34,44,45]. Like the DG methods, WG-FEM makes use of discontinuous functions in the finite element procedure which endows WG-FEMs with high flexibility to deal with geometric complexities and boundary conditions. For interface problems, such a flexibility gives rise to robustness in the enforcement of interface jump conditions. Unlike DG methods, WG-FEM enforces only weak continuity of variables naturally through well defined discrete differential operators. Therefore, weak Galerkin methods avoid pending parameters resulted from the excessive flexibility given to individual elements. As a consequence, WG-FEMs are absolutely stable once properly constructed. Recently, WG-FEMs have been applied to the solution of second-order elliptic equations [26], and the solution of Helmholtz equations with large wave numbers [27]. A major advantage of the present weak formulation is that it naturally enables WG-FEM to handle interface problems with low solution regularities. We demonstrate that the present WG-FEM of the lowest order is able to achieve from 1.75th order to second order of convergence in the solution and about first order of convergence in the gradient when the solution of the elliptic equation is C^1 or H^2 continuous and the interface is C^1 or Lipschitz continuous.

The rest of this paper is organized as follows. Section 2 is devoted to a description of the method and algorithm. We shall design a weak Galerkin formulation for the elliptic interface problem given in Eqs. (1.1)–(1.6). Section 3 is devoted to a convergence analysis for the weak Galerkin scheme presented in Section 2. In Section 4, we shall present some numerical results for several test cases in order to demonstrate the performance of the proposed WG-FEM for elliptic interface problems in 2D. We employ piecewise constant WG-FEMs, although piecewise linear WG-FEMs are also implemented. We first consider a few popular benchmark test examples with smooth but complex interfaces. We then carry out some investigation about nonsmooth interfaces. Some of these test problems admit solutions with low regularities, for which our numerical results significantly improve the best known result in literature and are better than our theoretical prediction. This paper ends with a conclusion, in which remarks on the use and possible advantages of high order WG-FEMs are given.

2. Methods and algorithms

Let $\mathcal{T}_h$ be a partition of the domain Ω with mesh size h. We require that the edges of the elements in $\mathcal{T}_h$ align with the interface Γ. Thus, the partition $\mathcal{T}_h$ can be grouped into two sets of elements denoted by $\mathcal{T}_h^1 = \mathcal{T}_h \cap \Omega_1$ and $\mathcal{T}_h^2 = \mathcal{T}_h \cap \Omega_2$,

respectively. Observe that $\mathcal{T}_h^j$ provides a finite element partition for the subdomain $\Omega_j, j = 1, 2$. The intersection of the partition $\mathcal{T}_h$ also introduces a finite element partition for the interface Γ, which shall be denoted by Γ_h. For simplicity, we adopt the following notation:

$$(v, w)_K := \int_K vwdK, \quad \langle v, w\rangle_{\partial K} := \int_{\partial K} vwds.$$

For each triangle $K \in \mathcal{T}_h$, let K^0 and ∂K denote the interior and boundary of K respectively. Denote by $P_j(K^0)$ the set of polynomials in K^0 with degree no more than j, and $P_\ell(e)$ the set of polynomials on each segment (edge or face) $e,\ e \in \partial K$ with degree no more than ℓ. A discrete function $w = \{w_0, w_b\}$ refers to a polynomial with two components in which the first component w_0 is associated with the interior K_0 and w_b is defined on each edge or face $e, e \in \partial K$. Please note that w_b may or may not equal to w_0, if the latter was extended to be defined on ∂K as well. Now we introduce three trial finite element spaces as follows

$$U_h := \left\{w = \{w_0, w_b\} :\ \{w_0, w_b\}|_K \in P_j(K^0) \times P_\ell(e),\ e \in \partial K,\ \forall K \in \mathcal{T}_h^1\right\}, \tag{2.1}$$

$$V_h := \left\{\rho = \{\rho_0, \rho_b\} :\ \{\rho_0, \rho_b\}|_K \in P_j(K^0) \times P_\ell(e),\ e \in \partial K,\ \forall K \in \mathcal{T}_h^2\right\}, \tag{2.2}$$

$$\Lambda_h := \left\{\mu :\ \mu|_e \in P_m(e),\ e \in \Gamma_h\right\}. \tag{2.3}$$

Define two test spaces by

$$U_h^0 := \{w = \{w_0, w_b\} \in U_h :\ w_b|_e = 0,\ \text{for } e \in \partial\Omega_1 \setminus \Gamma\}$$

and

$$V_h^0 := \{\rho = \{\rho_0, \rho_b\} \in V_h :\ \rho_b|_e = 0,\ \text{for } e \in \partial\Omega_2 \setminus \Gamma\}.$$

For each $w = \{w_0, w_b\} \in U_h$ or V_h, we define the discrete gradient of w, denoted by $\nabla_d w \in V_r(K)$ on each element K, by the following equation:

$$\int_K \nabla_d w \cdot q dK = -\int_K w_0(\nabla \cdot q)dK + \int_{\partial K} w_b(q \cdot \mathbf{n})ds, \quad \forall q \in V_r(K), \tag{2.4}$$

where $V_r(K)$ is a subspace of the set of vector-valued polynomials of degree no more than r on K.

The selection of the indices $j,\ \ell,\ m$, and r is critical in the design of weak Galerkin finite element methods. A detailed discussion on the selection of those indices can be found in [34]. In the present study of the interface problem, we shall let $j = \ell = m = k \geqslant 0$ in (2.1)–(2.3) and chose the Raviart–Thomas element for $V_r(K) := RT_k(K)$. These elements are referred as $\left\{P_k(K^0)^2,\ P_k(e)^2,\ P_k(\Gamma)\right\}$ elements in our numerical experiments. An exploration of other possible combinations is left to interested readers for future research. Recall that the Raviart–Thomas element [32] $RT_k(K)$ of order k is of the following form

$$RT_k(K) = P_k(K)^2 + \tilde{P}_k(K)\mathbf{x},$$

where $\tilde{P}_k(K)$ is the set of homogeneous polynomials of degree k and $\mathbf{x} = (x_1, x_2)$.

Weak Galerkin Algorithm 1. A numerical approximation for (1.1) – (1.6) can be obtained by seeking $u_h = \{u_0, u_b\} \in U_h$ satisfying $u_b = Q_b g_1$ on $\partial\Omega_1 \setminus \Gamma$, $v_h = \{v_0, v_b\} \in V_h$ satisfying $v_b = Q_b g_2$ on $\partial\Omega_2 \setminus \Gamma$ and $\lambda_h \in \Lambda_h$ such that

$$(A\nabla_d u_h, \nabla_d w) - \langle \lambda_h, w_b\rangle_\Gamma = (f_1, w_0), \quad \forall w \in U_h^0 \tag{2.5}$$

$$(A\nabla_d v_h, \nabla_d \rho) + \langle \lambda_h, \rho_b\rangle_\Gamma = (f_2, \rho_0) + \langle \psi, \rho_b\rangle_\Gamma, \quad \forall \rho \in V_h^0 \tag{2.6}$$

$$\langle u_b - v_b, \mu\rangle_\Gamma = \langle \phi, \mu\rangle_\Gamma, \quad \forall \mu \in \Lambda_h. \tag{2.7}$$

Here $Q_b g_1$ and $Q_b g_2$ are the standard L^2 projection of the Dirichlet boundary data in $P_k(e)$ for any edge/face $e \in \partial\Omega$.

3. Convergence theory

The goal of this section is to provide a convergence theory for the weak Galerkin finite element method as described in the previous section. First, we show that the WG algorithm has one and only one solution in the corresponding finite element trial space.

Lemma 3.1. *The weak Galerkin finite element method (2.5) – (2.7) has a unique solution.*

Proof. It suffices to show that the solution of (2.5)–(2.7) is trivial when data is homogeneous; i.e., $f_1 = f_2 = g_1 = g_2 = \phi = \psi = 0$. To this end, by letting $\mu = u_b - v_b$ in (2.7) and then using the assumption of $\phi = 0$ we obtain $u_b = v_b$ on Γ. Next, by first letting $w = u_h$ in (2.5) and $\rho = v_h$ in (2.6) and then adding them up gives

$$(A\nabla_d u_h, \nabla_d u_h) + (A\nabla_d v_h, \nabla_d v_h) = 0,$$

which implies $\nabla_d u_h = 0$ and $\nabla_d v_h = 0$. Thus, both u_h and v_h are constants over Ω_1 and Ω_2, respectively. It follows from the assumption of $u_b = 0$ on the non-empty set $\partial\Omega_1 \setminus \Gamma$ that $u_h = \{u_0, u_b\} = 0$. Thus, we have $v_b = u_b = 0$ on Γ, which together with $\nabla_d v_h = 0$ implies $v_h = 0$. Finally, using $\nabla_d u_h = 0$ and letting $w_b = \lambda_h$ on any edge/face $e \in \Gamma_h$, we have from Eq. (2.5) that

$$\langle \lambda_h, \lambda_h \rangle_\Gamma = 0,$$

which implies $\lambda_h = 0$. □

Denote by $Q_h = \{Q_0, Q_b\}$ a local L^2 projection operator where:

$$Q_0 : H^1(K^0) \to P_k(K^0), \quad Q_b : H^{\frac{1}{2}}(e) \to P_k(e), \quad e \in \partial K$$

are the usual L^2 projections into the corresponding spaces. Let Π_h be the usual projection operator in the mixed finite element method such that $\Pi_h \mathbf{q} \in H(\mathrm{div}, \Omega_i)$; and on each $K \in \mathcal{T}_h^i$, one has $\Pi_h \mathbf{q} \in RT_k(K)$ satisfying

$$(\nabla \cdot \mathbf{q},\ w_0)_K = (\nabla \cdot \Pi_h \mathbf{q},\ w_0)_K, \quad \forall w_0 \in P_k(K^0).$$

Lemma 3.2. *Let $\tau \in H(div, \Omega_i)$ be a smooth vector-valued function and Π_h be the locally defined projection operator commonly used in the mixed finite element method. Then, the following identify holds true*

$$\sum_{K \in \mathcal{T}_h^i} (-\nabla \cdot \tau,\ w_0)_K = \sum_{K \in \mathcal{T}_h^i} (\Pi_h \tau,\ \nabla_d w)_K - \langle w_b,\ \tau \cdot \mathbf{n} \rangle_\Gamma \tag{3.1}$$

for any $w = \{w_0, w_b\} \in V$ with $V = U_h^0$ or V_h^0 and $i = 1, 2$.

Proof. It follows from the definition of Π_h and ∇_d that

$$\sum_{K \in \mathcal{T}_h^i} (-\nabla \cdot \tau,\ w_0)_K = \sum_{K \in \mathcal{T}_h^i} (-\nabla \cdot \Pi_h \tau,\ w_0)_K = \sum_{K \in \mathcal{T}_h^i} \big((\Pi_h \tau,\ \nabla_d w)_K - \langle w_b,\ \Pi_h \tau \cdot \mathbf{n} \rangle_{\partial K} \big).$$

Now using the continuity of $\Pi_h \tau \cdot \mathbf{n}$ across each interior edge or face we arrive at

$$\sum_{K \in \mathcal{T}_h^i} (-\nabla \cdot \tau,\ w_0)_K = \sum_{K \in \mathcal{T}_h^i} (\Pi_h \tau,\ \nabla_d w)_K - \langle w_b,\ \Pi_h \tau \cdot \mathbf{n} \rangle_{\partial \Omega_i} = \sum_{K \in \mathcal{T}_h^i} (\Pi_h \tau,\ \nabla_d w)_K - \langle w_b,\ \tau \cdot \mathbf{n} \rangle_\Gamma,$$

where we have used the fact that $\langle w_b,\ \Pi_h \tau \cdot \mathbf{n} \rangle_\Gamma = \langle w_b,\ \tau \cdot \mathbf{n} \rangle_\Gamma$ and $w_b = 0$ on $\partial\Omega_i \setminus \Gamma$. This completes the proof. □

The following error estimates are straightforward from the definition of Π_h and Q_h. Readers can also find a verification of the result in [34].

Lemma 3.3. *For $u \in H^{k+2}(\Omega_1)$ and $v \in H^{k+2}(\Omega_2)$ with $k \geqslant 0$, we have*

$$\|\Pi_h(A\nabla u) - A\nabla_d(Q_h u)\| \leqslant Ch^{k+1} \|u\|_{k+2,\Omega_1}, \tag{3.2}$$

$$\|\Pi_h(A\nabla v) - A\nabla_d(Q_h v)\| \leqslant Ch^{k+1} \|v\|_{k+2,\Omega_2}. \tag{3.3}$$

It is well known that there exists a constant C such that for any function $g \in H^1(K)$

$$\|g\|_e^2 \leqslant C\Big(h_K^{-1} \|g\|_K^2 + h_K \|g\|_{1,K}^2 \Big), \tag{3.4}$$

where e is an edge of K.

Theorem 3.4. *Let $(u_h, v_h, \lambda_h) \in U_h \times V_h \times \Lambda_h$ be the solution arising from the weak Galerkin finite element scheme (2.5)–(2.7). Then, the following error estimates hold true*

$$\|\nabla_d(Q_h u - u_h)\| + \|\nabla_d(Q_h v - v_h)\| \leqslant Ch^{k+1}(\|u\|_{k+2} + \|v\|_{k+2}), \tag{3.5}$$

$$\|A\nabla u \cdot \mathbf{n} - \lambda_h\|_\Gamma \leqslant Ch^{k+\frac{1}{2}}(\|u\|_{k+2} + \|v\|_{k+2}), \tag{3.6}$$

where C stands for a generic constant independent of the mesh size h.

Proof. For simplicity, we assume that the coefficient A is a constant tensor on each element K. The proof can be extended to the general case of non-constant tensor A without any difficulty.

Now testing (1.1) with $w \in U_h^0$ and then using (3.1) leads to

$$(\Pi_h(A\nabla u),\ \nabla_d w) - \langle A\nabla u \cdot \mathbf{n},\ w_b \rangle_\Gamma = (f_1,\ w_0).$$

Adding the term $(A\nabla_d Q_h u,\ \nabla_d w)$ to both sides of the equation above, we obtain

$$(A\nabla_d Q_h u,\ \nabla_d w) - \langle A\nabla u\cdot\mathbf{n},\ w_b\rangle_\Gamma = (f_1,\ w_0) - (\Pi_h(A\nabla u) - A\nabla_d Q_h u,\ \nabla_d w). \tag{3.7}$$

Similarly, on Ω_2 we have for any $\rho \in V_h^0$ the following relation

$$(A\nabla_d Q_h v,\ \nabla_d \rho) - \langle A\nabla v\cdot\mathbf{n},\ \rho_b\rangle_\Gamma = (f_2,\ \rho_0) - (\Pi_h(A\nabla v) - A\nabla_d Q_h v,\ \nabla_d \rho). \tag{3.8}$$

Using the interface condition (1.6), (3.8) can be rewritten as

$$(A\nabla_d Q_h v,\ \nabla_d \rho) + \langle A\nabla u\cdot\mathbf{n},\ \rho_b\rangle_\Gamma = (f_2,\ \rho_0) + \langle \psi,\ \rho_b\rangle_\Gamma - (\Pi_h(A\nabla v) - A\nabla_d Q_h v,\ \nabla_d \rho). \tag{3.9}$$

Testing the interface condition (1.5) by $\mu \in \Lambda_h$ implies

$$\langle Q_b u - Q_b v,\ \mu\rangle_\Gamma = \langle u - v,\ \mu\rangle_\Gamma = \langle \phi,\ \mu\rangle_\Gamma. \tag{3.10}$$

For simplicity, we introduce the following notations to represent the errors:

$$\begin{aligned} e_h^u &\equiv \{e_0^u,\ e_b^u\} := \{Q_0 u - u_0, Q_b u - u_b\},\\ e_h^v &\equiv \{e_0^v,\ e_b^v\} := \{Q_0 v - v_0, Q_b v - v_b\},\\ \epsilon_u &:= Q_b(A\nabla u\cdot\mathbf{n}) - \lambda_h. \end{aligned}$$

Thus, the difference of (3.7) and (2.5) gives

$$(A\nabla_d e_h^u,\ \nabla_d w) - \langle \epsilon_u,\ w_b\rangle_\Gamma = -(\Pi_h(A\nabla u) - A\nabla_d Q_h u,\ \nabla_d w). \tag{3.11}$$

The difference of (3.9) and (2.6) gives

$$(A\nabla_d e_h^v,\ \nabla_d \rho) + \langle \epsilon_u,\ \rho_b\rangle_\Gamma = -(\Pi_h(A\nabla v) - A\nabla_d Q_h v,\ \nabla_d \rho). \tag{3.12}$$

The difference of (3.10) and (2.7) gives

$$\langle e_b^u - e_b^v,\ \mu\rangle_\Gamma = 0, \quad \forall \mu \in \Lambda_h. \tag{3.13}$$

First letting $w = e_h^u$ and $\rho = e_h^v$ in (3.11) and (3.12) and then adding them up gives

$$\|A^{\frac{1}{2}}\nabla_d e_h^u\|^2 + \|A^{\frac{1}{2}}\nabla_d e_h^v\|^2 = -(\Pi_h(A\nabla u) - A\nabla_d Q_h u,\ \nabla_d e_h^u) - (\Pi_h(A\nabla v) - A\nabla_d Q_h v,\ \nabla_d e_h^v).$$

Using (3.2) and (3.3), we have from the above equation that

$$\begin{aligned} C(\|\nabla_d e_h^u\| + \|\nabla_d e_h^v\|)^2 &\leqslant \|A^{\frac{1}{2}}\nabla_d e_h^u\|^2 + \|A^{\frac{1}{2}}\nabla_d e_h^v\|^2 \leqslant \|\Pi_h(A\nabla u) - A\nabla_d Q_h u\|\ \|\nabla_d e_h^u\| + \|\Pi_h(A\nabla v) - A\nabla_d Q_h v\|\ \|\nabla_d e_h^v\|\\ &\leqslant Ch^{k+1}(\|u\|_{k+2} + \|v\|_{k+2})(\|\nabla_d e_h^u\| + \|\nabla_d e_h^v\|), \end{aligned}$$

which implies

$$\|\nabla_d e_h^u\| + \|\nabla_d e_h^v\| \leqslant Ch^{k+1}(\|u\|_{k+2} + \|v\|_{k+2}). \tag{3.14}$$

Using (3.4) and the inverse inequality, we have for any edge or face $e \subset \Gamma \cap \partial K$

$$\|A\nabla_d e_h^u\cdot\mathbf{n}\|_e^2 \leqslant Ch^{-1}\|\nabla_d e_h^u\|_K^2, \tag{3.15}$$

$$\|(\Pi_h(A\nabla u) - A\nabla_d Q_h u)\cdot\mathbf{n}\|_e^2 \leqslant Ch^{-1}\|\Pi_h(A\nabla u) - A\nabla_d Q_h u\|_K^2. \tag{3.16}$$

Choosing $w = \{w_0, w_b\}$ in Eq. (3.11) such that $w_0 = 0$ for all $K \in \mathcal{T}_h^1$ and $w_b = \epsilon_u$ for $e \in \Gamma$ and $w_b = 0$ otherwise yields

$$\|\epsilon_u\|_\Gamma^2 = (A\nabla_d e_h^u,\ \nabla_d w) + (\Pi_h(A\nabla u) - A\nabla_d Q_h u,\ \nabla_d w).$$

Using (2.4), the equation above becomes

$$\|\epsilon_u\|_\Gamma^2 = \sum_{e\in\Gamma}(\langle A\nabla_d e_h^u\cdot\mathbf{n},\ \epsilon_u\rangle_e + \langle(\Pi_h(A\nabla u) - A\nabla_d Q_h u)\cdot\mathbf{n},\ \epsilon_u\rangle_e).$$

Using (3.15), (3.16), (3.2) and (3.5), we have

$$\begin{aligned} \|\epsilon_u\|_\Gamma^2 &\leqslant C\sum_{e\in\Gamma}(\|A\nabla_d e_h^u\cdot\mathbf{n}\|_e\|\epsilon_u\|_e + \|(\Pi_h(A\nabla u) - A\nabla_d Q_h u)\cdot\mathbf{n}\|_e\|\epsilon_u\|_e)\\ &\leqslant C\left(\sum_{K\in\mathcal{T}_h^1} h^{-1}\|\nabla_d e_h^u\|_K^2 + \sum_{K\in\mathcal{T}_h^1} h^{-1}\|\Pi_h(A\nabla u) - A\nabla_d Q_h u\|_K^2\right)^{1/2}\|\epsilon_u\|_\Gamma \leqslant Ch^{k+\frac{1}{2}}(\|u\|_{k+2} + \|v\|_{k+2})\|\epsilon_u\|_\Gamma, \end{aligned}$$

which verifies the error estimate (3.6). This completes the proof of the theorem. □

Table 4.1
Numerical convergence of the piecewise constant WG-FEM in L_2 norm for Example 1.

Mesh	max{h}	Solution		Gradient	
		L_2 error	Order	L_2 error	Order
Level 1	2.8553e−1	7.7581e−3		5.5883e−2	
Level 2	1.5110e−1	2.1194e−3	2.0390	2.7401e−2	1.1199
Level 3	7.7543e−2	5.3392e−4	2.0666	1.3738e−2	1.0349
Level 4	3.9258e−2	1.3374e−4	2.0338	6.8734e−3	1.0174
Level 5	1.9749e−2	3.3451e−5	2.0170	3.4373e−3	1.0086

Table 4.2
Numerical convergence of the piecewise constant WG-FEM in L_∞ norm for Example 1.

Mesh	max{h}	Solution		Gradient	
		L_∞ error	Order	L_∞ error	Order
Level 1	2.8553e−1	1.0266e−2		1.3042e−2	
Level 2	1.5110e−1	2.9631e−3	1.9525	6.5234e−3	1.0886
Level 3	7.7543e−2	7.6763e−4	2.0247	3.2615e−3	1.0391
Level 4	3.9258e−2	1.9518e−4	2.0118	1.6306e−3	1.0185
Level 5	1.9749e−2	4.9198e−5	2.0058	8.1523e−4	1.0090

4. Numerical experiments

The goal of this section is to numerically validate the proposed WG algorithm by solving some benchmark elliptic interface problems for which analytical solutions are known. To fully demonstrate the accuracy and robustness of the WG method, we consider challenging problems involving Lipschitz continuous interfaces, highly oscillated solutions, and solutions with low regularities. For simplicity, we focus on the piecewise constant WG-FEM $P_0(\partial K) - P_0(K) - RT_0(K)$ on structured triangular meshes in all numerical experiments. The use of the piecewise linear WG-FEM $P_1(\partial K) - P_1(K) - RT_1(K)$ is also explored in one example. The mesh generation and computation are all conducted in the MATLAB environment. Since the analytical solutions are known for each test case, the nonhomogeneous terms f_1 and f_2 of the elliptic equations and the Dirichlet boundary data can be correspondingly derived. Moreover, the two interface jump conditions for the solution and the flux across the interface are calculated according to the given analytical solution. Numerical errors in the solution and its gradient are reported in L_∞ and/or L_2 norms. For problems with low regularity solutions, it is customary to report errors only in L_∞ norm [21].

Example 1. We first study a classical circular interface problem [42]. Consider a square domain $[-1,1]\times[-1,1]$ with a circular interface $r^2 = x^2 + y^2 = \frac{1}{4}$. The coefficient A is defined to be $A_1 = b$ and $A_2 = 2$, respectively on each subdomain, for $r > 0.5$ and $r \leqslant 0.5$. The analytical solution to the elliptic equation is given as

$$\begin{aligned} u(x,y) &= -\left[\tfrac{1}{4}\left(1 - \tfrac{1}{8b} - \tfrac{1}{b}\right) + \left(\tfrac{r^4}{2} + r^2\right)\right]\Big/ b \quad && r > 0.5 \\ v(x,y) &= -(x^2 + y^2 - 1) && r \leqslant 0.5. \end{aligned}$$

By choosing $b = 10$, the function and flux jumps are actually constants [42].

By using a uniform triangular mesh, the L_2 and L_∞ errors of the piecewise constant WG-FEM for the solution and its gradient are reported in Tables 4.1 and 4.2, respectively. Based on successive mesh refinements, the numerically detected convergence rates are also reported for both error measurements. It can be seen that the orders of convergence in both L_2 and L_∞ norms for the solution are about two, while the orders in both norms for the gradient are about one. This agrees with our theoretical estimates for the piecewise constant WG-FEM approximations.

Higher order of convergence can be achieved by using corresponding higher order finite elements in the present WG framework. To demonstrate this, we solve the present interface problem by using the piecewise linear WG-FEM. Numerical convergences are reported in Tables 4.3 and 4.4, respectively, for L_2 and L_∞ errors. It is clear that for these error norms, the rates of convergence for the solution and its gradient are three and two, respectively. These results again validate our theoretical estimates.

In Figs. 4.1 and 4.2, the WG solutions based on the piecewise constant and piecewise linear finite elements are depicted, respectively. We show results obtained by using mesh level 1 and mesh level 5. Based on mesh level 1, the piecewise constant WG-FEM solution clearly consists of piecewise constants in Fig. 4.1, whereas the piecewise linear WG-FEM solution in Fig. 4.2 appears to be continuous in each subdomain. As expected, much better numerical solutions are attained for both WG-FEMs at mesh level 5. For the piecewise linear WG-FEM solution, it now looks not only continuous, but also smooth in each subdomain. For the piecewise constant WG-FEM solution, it looks smooth in low curvature regions. However, for

Table 4.3
Numerical convergence of the piecewise linear WG-FEM in L_2 norm for Example 1.

Mesh	max{h}	Solution		Gradient	
		L_2 error	Order	L_2 error	Order
Level 1	2.8553e−1	5.7134e−3		1.9952e−2	
Level 2	1.5110e−1	7.9652e−4	3.0960	4.8637e−3	2.2180
Level 3	7.7543e−2	1.0228e−4	3.0768	1.2169e−3	2.0769
Level 4	3.9258e−2	1.2872e−5	3.0450	3.0529e−4	2.0315
Level 5	1.9749e−2	1.6117e−6	3.0242	7.6516e−5	2.0141

Table 4.4
Numerical convergence of the piecewise linear WG-FEM in L_∞ norm for Example 1.

Mesh	max{h}	Solution		Gradient	
		L_∞ error	Order	L_∞ error	Order
Level 1	2.8553e−1	6.7856e−3		1.6699e−1	
Level 2	1.5110e−1	9.4240e−4	3.1020	5.2283e−2	1.8247
Level 3	7.7543e−2	1.1880e−4	3.1044	1.3000e−2	2.0862
Level 4	3.9258e−2	1.5013e−5	3.0389	3.2558e−3	2.0340
Level 5	1.9749e−2	1.8815e−6	3.0228	8.1431e−4	2.0171

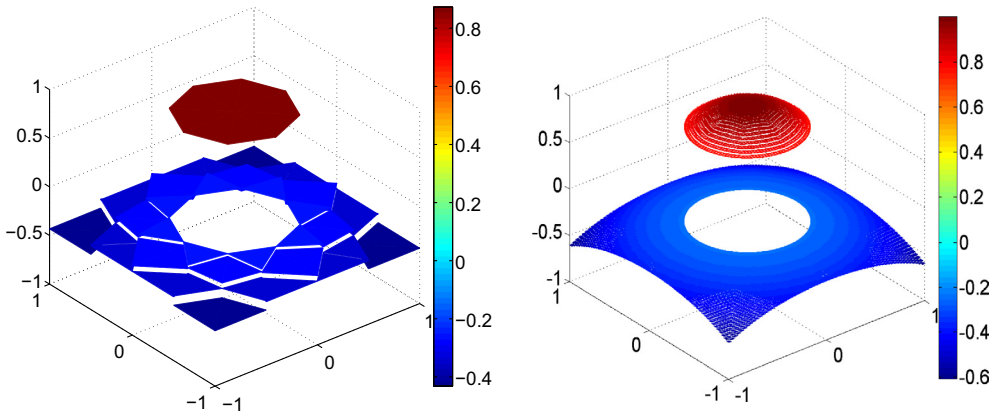

Fig. 4.1. The piecewise constant WG-FEM solutions of Example 1. Left: Mesh level 1; Right: mesh level 5.

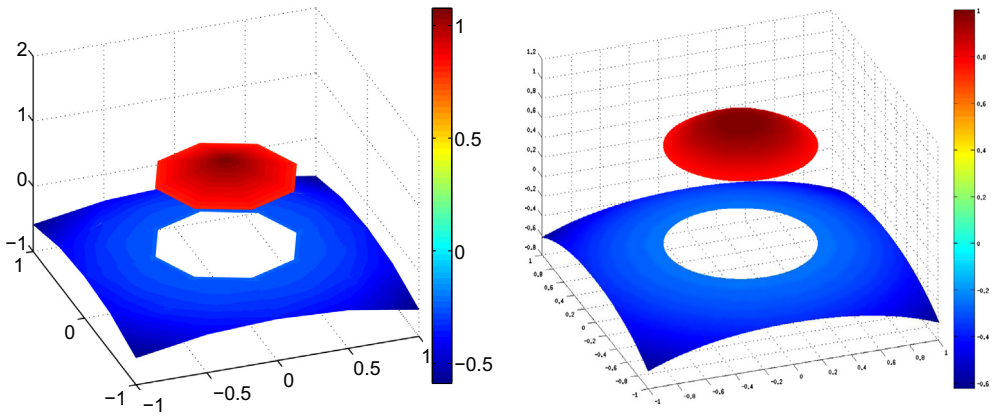

Fig. 4.2. The piecewise linear WG-FEM solutions of Example 1. Left: Mesh level 1; Right: mesh level 5.

Table 4.5
Numerical convergence in L_2 norm for Example 2 with $\kappa = 2$.

Mesh	max{h}	Solution		Gradient	
		L_2 error	Order	L_2 error	Order
Level 1	3.1778e−1	6.5483e−2		1.7052e−1	
Level 2	1.5889e−1	1.0989e−2	2.5751	8.2464e−2	1.0481
Level 3	7.9444e−2	2.5460e−3	2.1097	4.1494e−2	0.9908
Level 4	3.9722e−2	6.2538e−4	2.0254	2.0800e−2	0.9963
Level 5	1.9861e−2	1.5570e−4	2.0060	1.0408e−2	0.9989

Table 4.6
Numerical convergence in L_∞ norm for Example 2 with $\kappa = 2$.

Mesh	max{h}	Solution		Gradient	
		L_∞ error	Order	L_∞ error	Order
Level 1	3.1778e−1	7.6628e−2		1.5852e−1	
Level 2	1.5889e−1	1.5119e−2	2.3415	5.2258e−2	1.6009
Level 3	7.9444e−2	3.6142e−3	2.0646	2.0731e−2	1.3338
Level 4	3.9722e−2	8.9375e−4	2.0157	9.6505e−3	1.1031
Level 5	1.9861e−2	2.2492e−4	1.9905	4.7340e−3	1.0275

Table 4.7
Numerical convergence in L_∞ norm for Example 2 with $\kappa = 8$.

Mesh	max{h}	Solution		Gradient	
		L_∞ error	Order	L_∞ error	Order
Level 1	1.5837e−1	8.6774e−1		5.2751e−0	
Level 2	7.9186e−2	1.4156e−1	2.6159	9.1695e−1	2.5243
Level 3	3.9593e−2	2.3768e−2	2.5743	2.8679e−1	1.6768
Level 4	1.9796e−2	5.8719e−3	2.0170	1.0732e−1	1.4180
Level 5	9.8982e−3	1.4717e−3	1.9964	4.7255e−2	1.1834

high curvature regions, the piecewise constant solutions exhibit visible discontinuities. We note that such discontinuities are due to the nature of piecewise constant elements used in the WG-FEM. In other words, when the triangular mesh is not dense enough, the piecewise constant WG-FEM solution should display such visible discontinuities. When the mesh is dense enough, the piecewise constant WG-FEM solution is visually the same as the piecewise linear WG-FEM solution, or the analytical solution. Due to its reliable performance, we focus only on the piecewise constant WG-FEM in the rest of this paper.

Example 2. To further explore the potential of the proposed WG method, we consider a circular interface problem with highly oscillatory solutions. The high frequency or short wave solutions are commonly encountered in solving electromagnetic wave propagation and scattering problems governed by time domain Maxwell's equations or frequency domain Helmholtz equations. Here, we consider the following Helmholtz interface problem [42]

$$-\nabla\cdot(A_1\nabla u) - k_1^2 u = f_1 \quad r > 0.5, \tag{4.1}$$

$$-\nabla\cdot(A_2\nabla v) - k_2^2 v = f_2 \quad r \leqslant 0.5, \tag{4.2}$$

where the interface is still $r^2 = \frac{1}{4}$ over the domain $[-1,1]\times[-1,1]$. The wavenumber $k_i = \kappa\sigma_i$ $(i = 1,2)$ depends on the wavenumber κ of the wave solution in free space and dielectric profiles σ_i. In the present example, both A and σ_i are chosen to be discontinuous across the interface. In particular $A_1 = 1$ and $\sigma_1 = \sqrt{10}$ for $r > 0.5$ and $A_2 = 10$ and $\sigma_2 = 1$ for $r \leqslant 0.5$. The analytical solution is given as

$$\begin{aligned} u(x,y) &= -\sin(\kappa x)\cos(\kappa y) \quad && r > 0.5,\\ v(x,y) &= -(x^2+y^2) && r \leqslant 0.5. \end{aligned}$$

Other necessary interface jump conditions can be derived from the analytical solution.

The WG solution of the Helmholtz equation with high wavenumbers has been explored in [27]. For the present Helmholtz interface problem, a WG algorithm can be similarly constructed based on Eqs. (2.5)–(2.7). Two frequencies are tested, i.e., $\kappa = 2$ and $\kappa = 8$. For $\kappa = 2$, the WG errors in both L_2 and L_∞ norms are reported in Tables 4.5 and 4.6, respectively, while for $\kappa = 8$, only L_∞ errors are given in Table 4.7. By using $\kappa = 8$, the solution is of high frequency, see Fig. 4.3. In comparison with the numerical accuracy of the WG method for both cases, the WG errors for $\kappa = 8$ are larger even though a finer mesh is employed in the same mesh level. Nevertheless, when we examine the convergence rates, the WG method maintains the

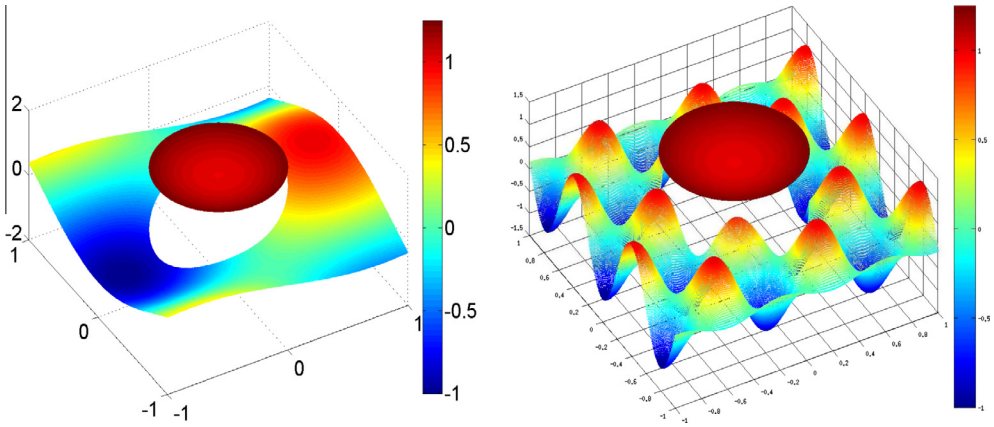

Fig. 4.3. WG solutions at mesh level 5 for Example 2. Left: $\kappa = 2$; Right: $\kappa = 8$.

Table 4.8
Numerical convergence in L_2 norm for Example 3 with $b = 10$.

Mesh	max{h}	Solution		Gradient	
		L_2 error	Order	L_2 error	Order
Level 1	5.6522e−1	1.6429e−1		4.9445e−1	
Level 2	2.8261e−1	2.8872e−2	2.5085	1.8400e−1	1.7590
Level 3	1.4130e−1	7.7717e−3	1.8933	9.0209e−2	0.9725
Level 4	7.0652e−2	1.4740e−3	2.3986	4.4790e−2	0.9900
Level 5	3.5326e−2	2.0128e−4	2.8725	2.2394e−2	0.9999

Table 4.9
Numerical convergence in L_∞ norm for Example 3 with $b = 10$.

Mesh	max{h}	Solution		Gradient	
		L_∞ error	Order	L_∞ error	Order
Level 1	5.6522e−1	1.4339e−1		1.5956e−1	
Level 2	2.8261e−1	2.6979e−2	2.4100	9.1557e−2	0.8014
Level 3	1.4130e−1	7.3332e−3	1.8792	5.8167e−2	0.6544
Level 4	7.0652e−2	1.4904e−3	2.2988	2.9623e−2	0.9735
Level 5	3.5326e−2	2.8124e−4	2.4058	1.5250e−2	0.9579

Table 4.10
Numerical convergence in L_∞ norm for Example 3 with $b = 1000$.

Mesh	max{h}	Solution		Gradient	
		L_∞ error	Order	L_∞ error	Order
Level 1	5.6522e−1	4.1482e−1		3.1081e−1	
Level 2	2.8261e−1	5.3753e−2	2.9481	1.0784e−1	1.5271
Level 3	1.4130e−1	1.3707e−2	1.9713	5.6088e−2	0.9431
Level 4	7.0652e−2	3.0677e−3	2.1598	2.9658e−2	0.9193
Level 5	3.5326e−2	6.2057e−4	2.3055	1.5204e−2	0.9640

same rates, i.e., second and first orders, respectively, for the solution and its gradient, in both cases. This verifies the capability of the WG method in resolving short wave problems.

Example 3. We next consider an example with a high contrast in coefficient A [42] to examine the robustness of the WG method. Consider the second order elliptic equation over the domain $[-1, 1] \times [-1, 1]$. The interface Γ is defined to be an ellipse

$$\left(\frac{x}{10/27}\right)^2 + \left(\frac{y}{18/27}\right)^2 = 1.$$

We set $A_2 = b$ inside of Γ, and $A_1 = 1$ outside of Γ. The analytical solution is given as

$$\begin{aligned} u(x,y) &= 5e^{-x^2-y^2} \quad \text{outside } \Gamma, \\ v(x,y) &= e^x \cos(y) \quad \text{inside } \Gamma. \end{aligned}$$

Related interface jump conditions can be derived from the analytical solution.

Two values of b are tested with $b = 10$ and $b = 1000$. The latter case involves a much larger jump in A. This results in a larger condition number for the corresponding discretized linear system. This means that extensive computational cost is usually needed in the matrix computation. The WG method performs robustly for both cases. For $b = 10$, both L_2 and L_∞ errors are presented in Tables 4.8 and 4.9, respectively. For $b = 1000$, only L_∞ errors are reported in Table 4.10. It can be seen from three tables that the convergence rates are first and second orders, respectively, for the gradient and the solution in L_2 and/or L_∞ norms. The WG solutions on mesh levels 1 and 5 are shown in Figs. 4.4 and 4.5, respectively, for $b = 10$ and $b = 1000$. We note that in both cases, the analytical solutions are the same and are independent of the coefficient A. Thus, even though there are some minor differences in the WG solutions at mesh level 1 for $b = 10$ and $b = 1000$, the WG solutions are visually identical at mesh level 5. This demonstrates the robustness of the WG method in handling elliptic interface problems with a high interface contrast.

Example 4. We next consider an interface with both concave and convex curve segments

$$\Gamma : \begin{cases} x(\theta) = 0.6\cos(\theta) - 0.3\cos(3\theta), \\ y(\theta) = 1.5 + 0.7\sin(\theta) - 0.07\sin(3\theta) + 0.2\sin(7\sin\theta). \end{cases}$$

over the domain $[-1,1] \times [0,3]$. The coefficient is chosen to be $A_1 = 10$ and $A_2 = 1$, respectively, for outside and inside Γ. The analytical solution is given as

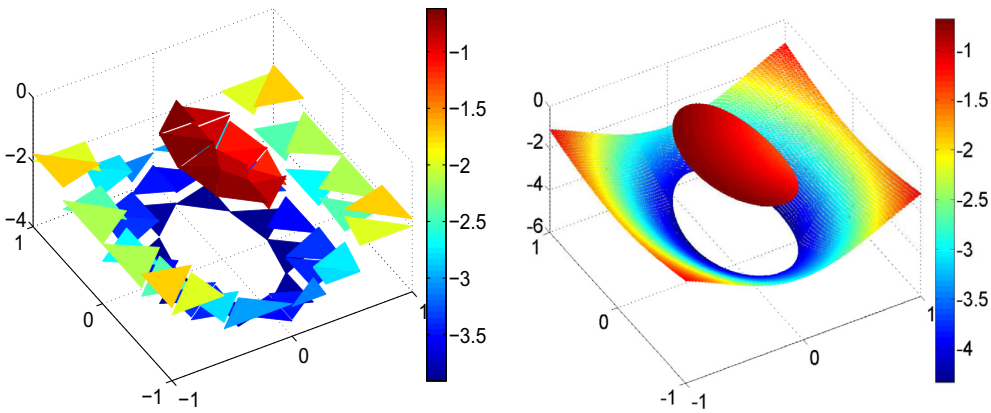

Fig. 4.4. WG solutions of Example 3 with $b = 10$. Left: Mesh level 1; Right: mesh level 5.

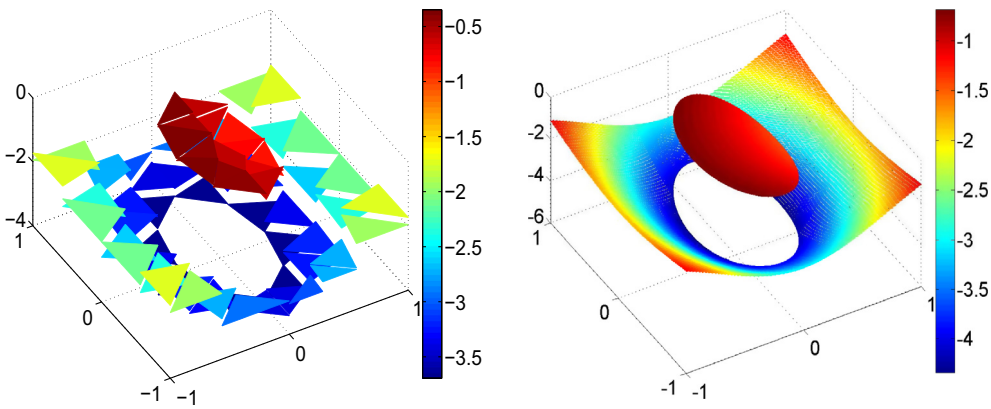

Fig. 4.5. WG solutions of Example 3 with $b = 1000$. Left: Mesh level 1; Right: mesh level 5.

$$u(x,y) = -x^2 - y^2 \qquad \text{outside } \Gamma$$
$$v(x,y) = e^x(y^2 + x^2\sin(y)) \qquad \text{inside } \Gamma$$

Other necessary interface jump conditions can be derived from the analytical solutions.

The L_2 errors of the WG FEM are listed in Table 4.11. It is clear that the WG method yields again the second and first orders of convergence, respectively, for the solution and its gradient. The WG solutions on mesh levels 1 and 5 are depicted in Fig. 4.6. The curvature change of the interface Γ in between positive and negative values can be clearly seen in the figure. The WG solutions are satisfactory in both mesh levels. In particular, for mesh level 5, the discontinuities can be observed in the upper left part of the H shape, while the solution is quite smooth in other parts.

Example 5. We next consider a classical elliptic interface problem with both concave and convex curve segments [42]. The interface Γ is parametrized with the polar angle θ

$$r = \frac{1}{2} + \frac{\sin(5\theta)}{7},$$

inside a square domain $[-1,1]\times[-1,1]$. The coefficient is chosen to be $A_1 = 10$ and $A_2 = 1$, respectively, for outside and inside Γ. The analytical solution is given as

$$u(x,y) = 0.1(x^2+y^2)^2 - 0.01\ln(2\sqrt{x^2+y^2}) \qquad \text{outside } \Gamma$$
$$v(x,y) = e^{x^2+y^2} \qquad \text{inside } \Gamma.$$

Related interface jump conditions can be derived from the analytical solutions.

The WG solutions and their convergence are reported in Table 4.12 and Fig. 4.7, respectively. It can be seen from the table that the convergence is of order two and one for the solution and its gradient, respectively, in the L_∞ norm. It should be pointed out that mesh quality plays an important role in the performance of general finite element methods. For weak Galerkin, we found that the quality of mesh affects the corresponding numerical approximation. For example, we noticed a slower convergence when the finite element partition consists of both acute and non-acute triangles with nontrivial portion. After eliminating most of the non-acute triangles, the WG approximation exhibits an improved rate of convergence numerically. Fig. 4.8 demonstrates some meshes generated by MATLAB in the present study after an elimination of most non-acute triangles through a numerical procedure. It can be seen that, at each level, the triangular mesh is fitted to the interface at the nodal points. Observe that these meshes are highly non-uniform and unstructured. In particular, it is clear that much smaller

Table 4.11
Numerical convergence test for Example 4.

Mesh	max{h}	Solution		Gradient	
		L_2 error	Order	L_2 error	Order
Level 1	4.3362e−1	1.2487e−2		3.8399e−1	
Level 2	2.6220e−1	4.9344e−3	1.8456	2.0277e−1	1.2693
Level 3	1.4915e−1	1.3051e−3	2.3574	1.0635e−1	1.1439
Level 4	7.6493e−2	3.8847e−4	1.8148	5.3770e−2	1.0214
Level 5	4.0765e−2	9.6391e−5	2.2146	2.6540e−2	1.2218

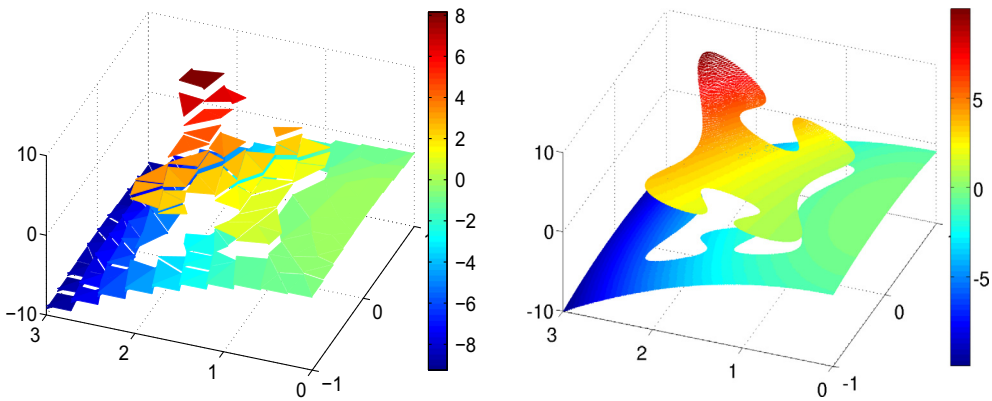

Fig. 4.6. WG solutions of Example 4. Left: Mesh level 1; Right: mesh level 5.

Table 4.12
Numerical convergence test for Example 5.

Mesh	max{h}	Solution		Gradient	
		L_∞ error	Order	L_∞ error	Order
Level 1	3.4726e−1	1.5885e−3		3.5260e−2	
Level 2	1.7363e−1	3.8053e−4	2.0616	1.6630e−2	1.0842
Level 3	8.9010e−2	9.1082e−5	2.1399	9.0379e−3	0.9126
Level 4	4.9602e−2	2.6778e−5	2.0936	5.0265e−3	1.0034
Level 5	2.4286e−2	5.9847e−6	2.0982	2.4459e−3	1.0087

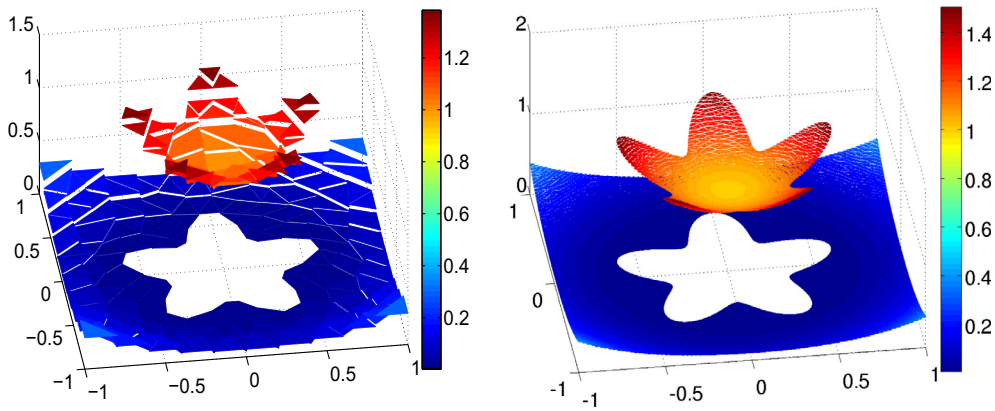

Fig. 4.7. WG solutions of Example 5. Left: Mesh level 1; Right: mesh level 5.

triangles are employed to resolve the concave portion of the interface. This somehow helped the WG method to deliver numerical solutions with high accuracy since the solution changes rapidly in regions with large curvatures.

For all examples in the rest of this paper, we study solutions with low regularities. It is customary to report only L_∞ errors for such studies in the literature [21]. Therefore, we only present L_∞ errors.

Example 6. In this and next two examples, we consider an interface problem with C^1 continuous interfaces as discussed in the literature [21]. The domain is given as $\Omega = [-1,1] \times [-1,1]$, and the interface Γ is defined with two pieces: $y = 2x$ for $x + y > 0$ and $y = 2x + x^2$, for $x + y \leqslant 0$. The interface Γ divides the domain into two parts Ω_1 and Ω_2. Here we denote Ω_1 and Ω_2, respectively, to be the part on the left and right of Γ. An inhomogeneous second order elliptic equation is considered, i.e., the coefficient A is not piecewise constant. Instead, we have $A_1(x,y) = (xy+2)/5$ in Ω_1 and $A_2(x,y) = (x^2 - y^2 + 3)/7$ in Ω_2. The analytical solution u is fixed to be $u = 2$ in Ω_1, while in Ω_2, v is defined piecewisely by

$$v(x,y) = \begin{cases} \sin(x+y), & \text{if } x+y \leqslant 0 \\ x+y, & \text{if } x+y > 0. \end{cases}$$

Other necessary conditions can be derived from the analytical form of the solution. In particular, the Dirichlet boundary data is derived for both $u = g$ and $v = g$, since in this example, Ω_2 is not enclosed by Ω_1.

A numerical investigation was conducted and the results are reported in Table 4.13. Again, the WG method attains the theoretical order of convergence for this example, i.e., first and second order of accuracy respectively for the gradient and the solution in L_∞ norm. We note that due to the piecewise definition, the solution $v(x,y)$ is C^2 continuous but not C^3 across the line $x + y = 1$. In our computation, the line $x + y = 1$ is not treated as a boundary. Thus, our triangulation is not aligned with this line. This can be seen clearly in the graph of the WG solution on mesh level 1 (Fig. 4.9 left). In the right chart of Fig. 4.9, a smooth transition can be seen across $x + y = 1$ in the WG solution on mesh level 5.

Example 7. Here we consider the same interface and domain geometry as in Example 6. The coefficient function $A(x,y)$ is defined in the same way as in Example 6. We also fix the solution as $u = 2$ in Ω_1. But in Ω_2, the solution is given differently by (see [21] for details)

$$v(x,y) = \begin{cases} \sin(x+y) + \cos(x+y), & \text{if } x+y \leqslant 0 \\ x+y+1, & \text{if } x+y > 0. \end{cases}$$

Other necessary conditions can be derived similarly. Observe that the solution $v = v(x,y)$ is C^1 continuous but not C^2 across the line $x + y = 1$.

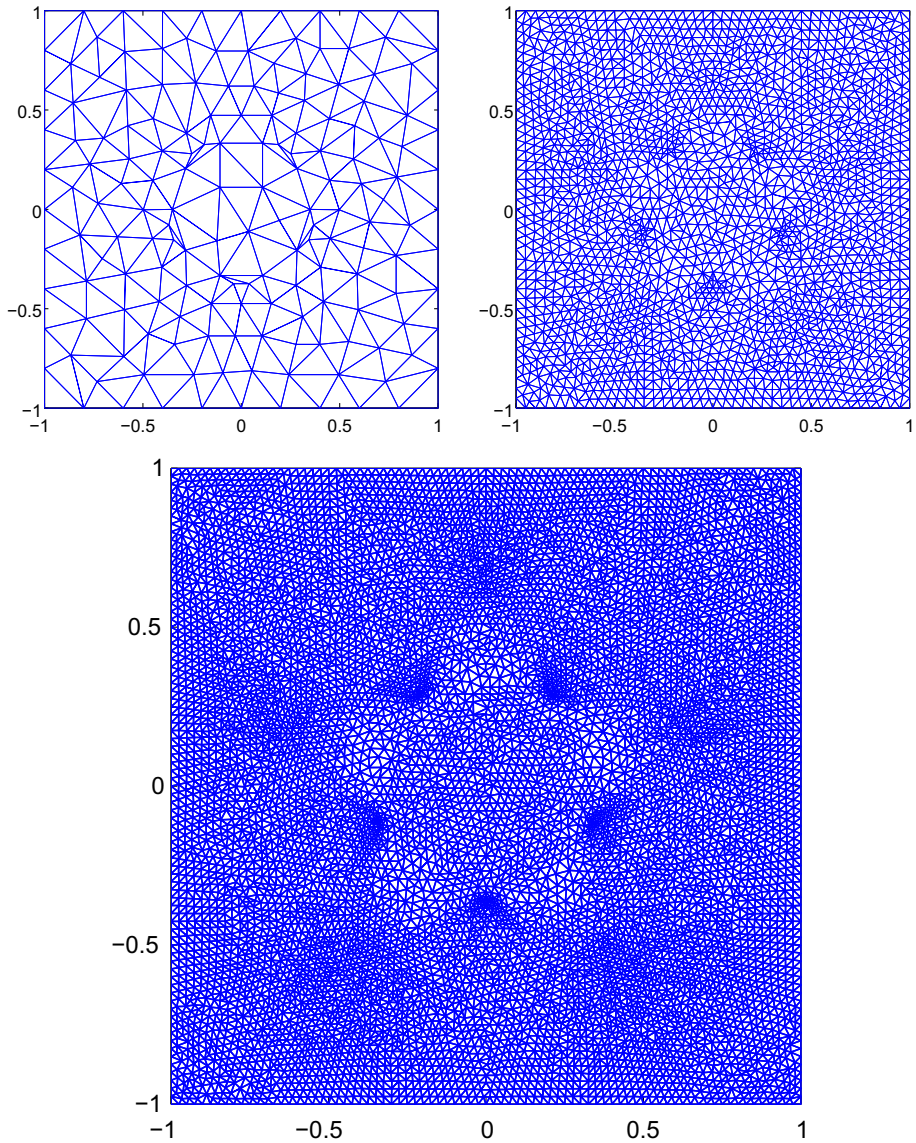

Fig. 4.8. Finite element meshes of Example 5. Top left: Mesh level 1; Top right: Mesh level 3; Bottom: Mesh level 5.

Table 4.13
Numerical convergence test for Example 6.

Mesh	max{h}	Solution		Gradient	
		L_∞ error	Order	L_∞ error	Order
Level 1	6.2575e−1	1.5275e−2		4.8833e−2	
Level 2	2.9662e−1	3.9259e−3	1.8200	3.1059e−2	0.6062
Level 3	1.5170e−1	1.0586e−3	1.9546	1.5584e−2	1.0285
Level 4	7.9102e−2	3.3419e−4	1.7707	8.0209e−3	1.0200
Level 5	4.4180e−2	1.1698e−4	1.8022	4.4282e−3	1.0199

The WG algorithm is formulated as in the previous example. In particular, since $v(x,y)$ is C^1 across $x+y=1$, the function and flux jumps are trivially zero across $x+y=1$. Thus, again, no special boundary or interface treatment is carried out near the line $x+y=1$. In fact, this line actually cuts through the finite element triangles; see the left chart of Fig. 4.10. It can be seen that the loss of regularity in $v(x,y)$ is visually indistinguishable in the WG solution on mesh level 5 (see the right chart of Fig. 4.10). In the literature, a certain reduction of convergence order has been reported for this C^1 continuous example [21]

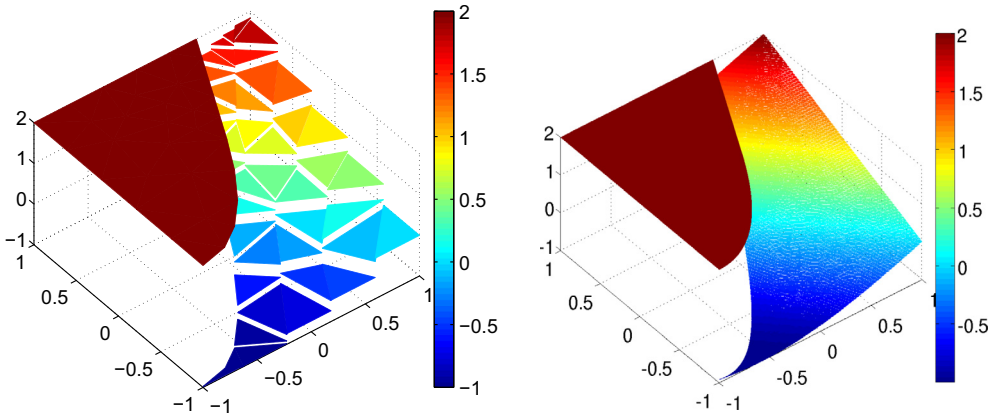

Fig. 4.9. WG solutions of Example 6. Left: Mesh level 1; Right: mesh level 5.

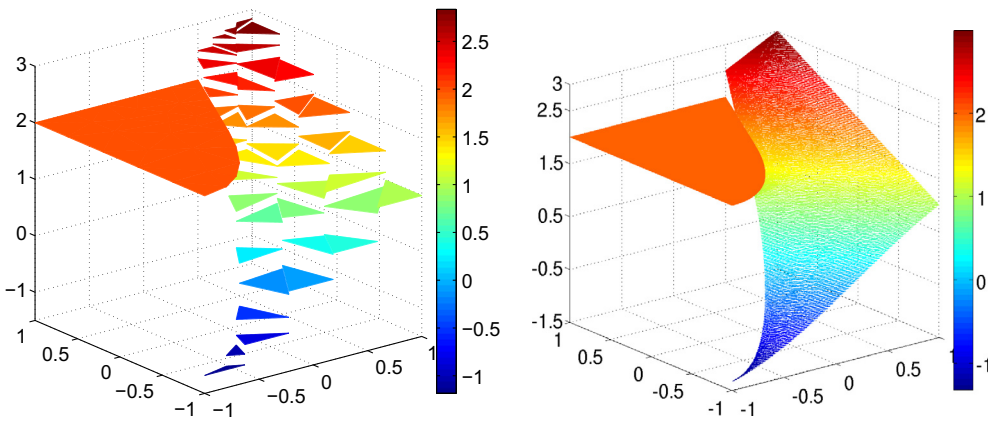

Fig. 4.10. WG solutions of Example 7. Left: Mesh level 1; Right: mesh level 5.

when the standard Galerkin finite element method is employed for a numerical approximation. In the present study, it is found that the order of convergence remains unchanged for the WG method, see Table 4.14. This indicates that the WG method preforms robustly for the challenging problem with low regularity.

Example 8. Consider again the same interface problem as in Examples 6 and 7, over a larger domain $\Omega = [-1,3] \times [-1,1]$. The coefficient function $A(x,y)$ is now defined to be $A_1(x,y) = 1$ in Ω_1 and $A_2(x,y) = 2 + \sin(x+y)$ in Ω_2. The analytical solution is give as [21]

$$\begin{aligned} u(x,y) &= 8 && \text{in } \Omega_1, \\ v(x,y) &= (x^2+y^2)^{5/6} + \sin(x+y) && \text{in } \Omega_2. \end{aligned}$$

Other necessary conditions can be derived from the analytical solutions.

The analytical solution is piecewise H^2 in this example. In particular, the function $v(x,y)$ has a singularity at $(0,0)$ with blow-up derivatives. Even though the analytical solution is well behaved in other places, the singularity at the origin may cause some order reduction in the finite element simulation [21]. Due to this singularity, the convergence rate of the WG method in the L_∞ norm of the solution is reduced to be about 1.75 for the present example, see Table 4.15. On the other hand, the order of convergence of the WG method for the gradient remains to be about one. The numerical solutions at mesh levels 1 and 5 are depicted in Fig. 4.11. Interestingly, in both levels, the singularity at the origin is invisible. But the numerical algorithm can sense this singularity via the convergence rate.

Example 9. In this and next two examples, we continue to examine the performance of the WG method for solutions of low regularity when the interface is fixed to be a Lipschitz continuous curve[21]. On a rectangular domain $\Omega = [-1,3] \times [-1,1]$, we consider a case where the interface Γ consists of two pieces: $y = 2x$ for $x + y > 0$ and $y = -x/2$, for $x + y \leqslant 0$. Thus, the

Table 4.14
Numerical convergence test for Example 7.

Mesh	max{h}	Solution		Gradient	
		L_∞ error	Order	L_∞ error	Order
Level 1	6.2575e−1	2.6559e−2		4.9273e−2	
Level 2	2.9662e−1	5.9674e−3	2.0001	2.8456e−2	0.7355
Level 3	1.5170e−1	1.5342e−3	2.0257	1.4493e−2	1.0062
Level 4	7.9102e−2	4.4127e−4	1.9137	7.5081e−3	1.0100
Level 5	4.4180e−2	1.5022e−4	1.8500	3.9584e−3	1.0990

Table 4.15
Numerical convergence test for Example 8.

Mesh	max{h}	Solution		Gradient	
		L_∞ error	Order	L_∞ error	Order
Level 1	6.5801e−1	3.4340e−2		3.2817e−1	
Level 2	3.4551e−1	1.1022e−2	1.7641	1.7896e−1	0.9413
Level 3	1.7932e−1	3.5197e−3	1.7405	9.5039e−2	0.9650
Level 4	9.1176e−2	1.0806e−3	1.7459	5.0095e−2	0.9468
Level 5	4.6365e−2	3.3092e−4	1.7499	2.6003e−2	0.9696

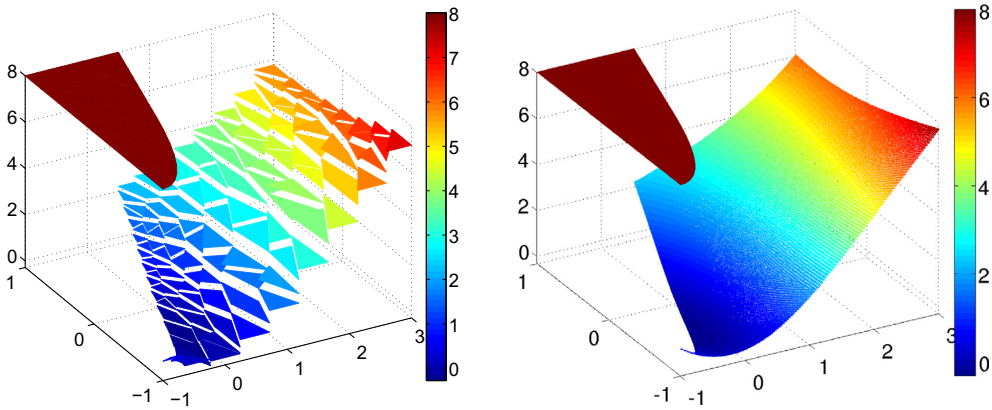

Fig. 4.11. WG solutions of Example 8. Left: Mesh level 1; Right: mesh level 5.

interface Γ has a kink at $(0,0)$. Denote by Ω_1 the region on the left and upper part of Γ, and Ω_2 to be the rest of the domain. The coefficient is given piecewisely by $A_1(x,y) = (xy+2)/5$ in Ω_1 and $A_2(x,y) = (x^2 - y^2 + 3)/7$ in Ω_2. The analytical solution u is fixed to be $u = 8$ in Ω_1, while in Ω_2, v is given piecewisely by

$$v(x,y) = \begin{cases} \sin(x+y), & \text{if } x+y \leqslant 0, \\ x+y, & \text{if } x+y > 0. \end{cases}$$

Other necessary conditions can be derived from the analytical solutions.

Similar to Example 6, the analytical solution is of C^2 continuous but not C^3 in this example. The WG method yields uniformly second and first order of accuracy in L_∞ norm, respectively, for the solution and its gradient as shown in Table 4.16. The kink of the interface Γ is clearly seen in both charts of Fig. 4.12. In particular, on the coarsest mesh, the alignment of finite element triangles to two line segments of Γ is obvious. No deterioration in solution occurs around the interface corner.

Example 10. Consider an elliptic problem with the same interface and domain geometry as in Example 9. The coefficient function $A(x,y)$ is defined the same as in Example 9. Also, we fix the solution to be $u = 8$ in Ω_1. But in Ω_2, the solution is given differently [21] by

$$v(x,y) = \begin{cases} \sin(x+y) + \cos(x+y), & \text{if } x+y \leqslant 0, \\ x+y+1, & \text{if } x+y > 0. \end{cases}$$

Table 4.16
Numerical convergence test for Example 9.

Mesh	max{h}	Solution		Gradient	
		L_∞ error	Order	L_∞ error	Order
Level 1	5.6919e−1	1.4984e−2		3.3001e−2	
Level 2	2.8459e−1	4.4307e−3	1.7578	1.7812e−2	0.8897
Level 3	1.4230e−1	1.2336e−3	1.7687	9.8402e−3	0.8561
Level 4	7.1149e−2	3.2639e−4	1.8634	5.1905e−3	0.9228
Level 5	3.5574e−2	8.5110e−5	1.9231	2.6699e−3	0.9591

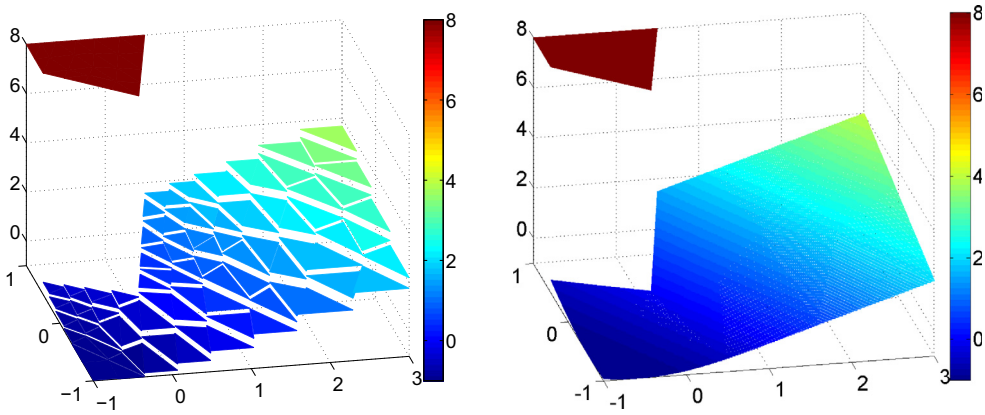

Fig. 4.12. WG solutions of Example 9. Left: Mesh level 1; Right: mesh level 5.

Other necessary conditions can be derived similarly. Like in Example 7, $v(x,y)$ is of C^1 continuous but not C^2 across the line $x+y=1$. Similarly, no special numerical treatment is invoked near the line $x+y=1$ so that this line actually cuts through finite element triangles, see the left chart of Fig. 4.13. It can be seen from Table 4.17 that the WG method converges uniformly with orders being close to second and first, respectively, for the solution and its gradient in the L_∞ norm. Technically speaking, the interface is Lipschitz continuous in this example, while it is C^1 continuous in Example 7. In other words, the interface regularity is lower here than that in Example 7. However, since body-fitted triangular meshes are employed in the WG method, the interface with two simple line segments in the present example is easier to be resolved by the body-fitted grids than the curved interface in Example 7. The only issue that could make an impact on the convergence is the geometrical singularity at the origin. The last and present examples show that the WG method is very robust in handling geometrical singularity, or sharp edged corners in general.

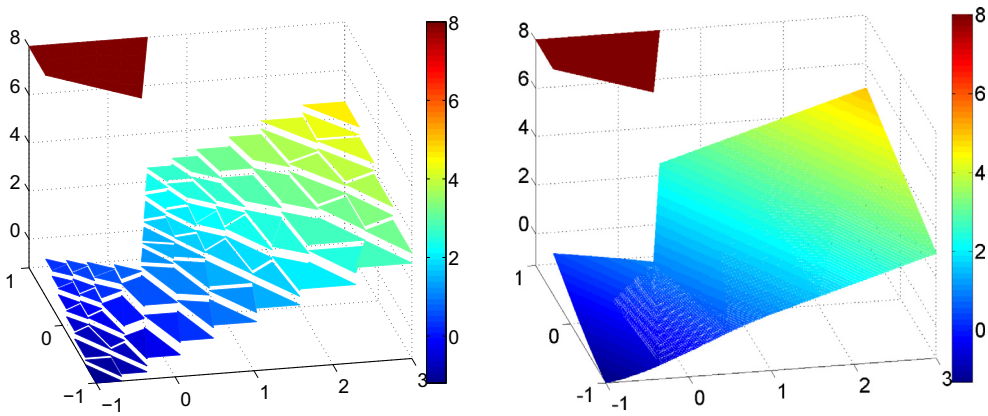

Fig. 4.13. WG solutions of Example 10. Left: Mesh level 1; Right: mesh level 5.

Table 4.17
Numerical convergence test for Example 10.

Mesh	max{h}	Solution		Gradient	
		L_∞ error	Order	L_∞ error	Order
Level 1	5.6919e−1	1.4326e−2		3.3514e−2	
Level 2	2.8459e−1	4.4250e−3	1.6949	2.0051e−2	0.7411
Level 3	1.4230e−1	1.2350e−3	1.8411	1.0768e−2	0.8968
Level 4	7.1149e−2	3.2693e−4	1.9175	5.5458e−3	0.9573
Level 5	3.5574e−2	8.5118e−5	1.9415	2.8004e−3	0.9858

Example 11. Consider the same interface and geometry as in Examples 9 and 10. The coefficient function $A(x,y)$ is now defined to be $A_1(x,y) = 1$ in Ω_1 and $A_2(x,y) = 2 + \sin(x+y)$ in Ω_2. The analytical solutions are give as [21]

$$\begin{aligned} u(x,y) &= 8 && \text{in } \Omega_1, \\ v(x,y) &= (x^2+y^2)^{5/6} + \sin(x+y) && \text{in } \Omega_2. \end{aligned}$$

Other necessary conditions can be derived from the analytical solution.

Similar to Example 8, the analytical solution is piecewise H^2 in the present case. The solution $v(x,y)$ has a singularity at $(0,0)$ with blow-up derivatives. The WG method achieves a similar order of accuracy as that in Example 8. In particular, it can be seen in Table 4.18 that the L_∞ error in the solution is of order 1.75, while it remains to be about one for the gradient approximation. Both function singularity and geometrical singularity are presented at the origin in this test; see the WG solutions in Fig. 4.14. Nevertheless, the WG method is capable of delivering decent results at mesh level 1.

Finally, we summarize the WG results from Example 6 to Example 11 in Table 4.19. In each case, an overall convergence rate is reported, which is calculated based only on mesh level 1 and level 5. It can be seen from the L_∞ error of the gradient that the WG method essentially attains the first order of accuracy in all test cases. For the L_∞ error of the solution, we analyze the order of the WG method case by case. When the solution is C^2 continuous, the loss of regularity has no impact on the order of convergence regardless whether the interface is C^1 continuous or Lipschitz continuous. When the solution is C^1 continuous, the WG method achieves a very good order of accuracy for C^1 continuous interface, while such order is slightly reduced when the interface is Lipschitz continuous. However, the overall order of convergence for the WG method for the latter case is still very close to two. Thus, it is fair to say that the WG method attains a second order of accuracy in L_∞ norm

Table 4.18
Numerical convergence test for Example 11.

Mesh	max{h}	Solution		Gradient	
		L_∞ error	Order	L_∞ error	Order
Level 1	7.1020e−1	4.0630e−2		7.1308e−2	
Level 2	3.5510e−1	1.1389e−2	1.8349	4.0849e−2	0.8038
Level 3	1.7755e−1	3.3569e−3	1.7624	2.1170e−2	0.9483
Level 4	8.8775e−2	1.0150e−3	1.7256	1.0780e−2	0.9737
Level 5	4.4387e−2	3.1128e−4	1.7052	5.5740e−3	0.9516

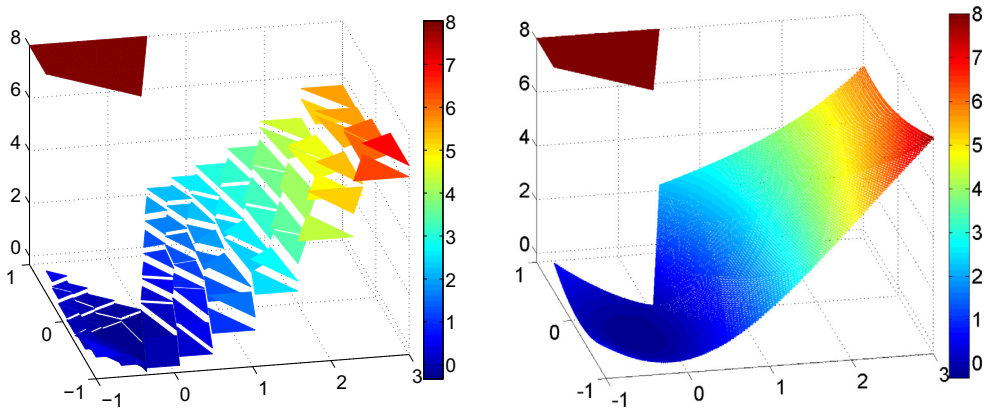

Fig. 4.14. WG solutions of Example 11. Left: Mesh level 1; Right: mesh level 5.

Table 4.19
Summary of the overall orders of the WG method for solutions with low regularities.

Regularity	Γ is C^1 continuous		Γ is Lipschitz continuous	
	Solution	Gradient	Solution	Gradient
C^2	1.8380	0.9056	1.8650	0.9069
C^1	1.9523	0.9513	1.8487	0.8953
H^2	1.7500	0.9558	1.7570	0.9193

for C^1 continuous solutions. On the other hand, the L_∞ error of the WG method is always around the order of 1.75 when the solution is H^2 continuous, for both C^1 and Lipschitz continuous interfaces. In other words, even though the geometrical singularity does not affect the convergence of the WG method, the function singularity may do. Nevertheless, we note that a 1.75th order for solution with low regularities is still some of the best for this class of challenging problems, to our best knowledge. Moreover, although not reported in detail in this paper, the WG method achieves the second order of accuracy in L_2 norm for the solution. Therefore, the present study demonstrates a good robustness of the WG method for solving elliptic interface problems. Readers are also encouraged to draw their own conclusions from the results reported in this paper.

5. Conclusion

The present paper presents some of the best results for solving two-dimensional (2D) elliptic partial differential equations (PDE) with low solution regularity resulted from modeling nonsmooth interfaces. The weak Galerkin finite element method (WG-FEM) of Wang and Ye [34] is introduced for this class of problems. The WG-FEM is a new approach that employs discontinuous functions in the finite element procedure to gain flexibility in enforcing boundary and interface conditions. Such a strategy is akin to that used by the discontinuous Galerkin (DG) methods. However, by enforcing only weak continuity of variables though well defined discrete differential operators, the WG-FEM is able to avoid pending parameters commonly occurred in the DG-FEMs. Like traditional FEMs, the WG-FEM employs body-fitted element meshes to represent boundaries and material interfaces. Such an approach is convenient for handling nonsmooth interfaces or geometric singularities. The convergence analysis of the present WG-FEM for elliptic interface problems is given. The validity of the WG-FEM is further tested over a large number of benchmark numerical tests with various complex interface geometries and nonsmooth interfaces. For problems with smooth interfaces and sufficient solution regularities, the designed third and second orders of accuracy are numerically confirmed, respectively, for the piecewise linear and piecewise constant WG-FEMs.

Nonsmooth interfaces, such as sharp edges, cusps, and tips are ubiquitous both in nature and in engineering devices and structures. When nonsmooth interfaces are associated with elliptic PDEs, they result in difficulties in theoretical analysis and in the design of numerical algorithms. Unfortunately, to tackle the real-world problems, dealing with nonsmooth interfaces is not avoidable in scientific computing. What aggravates the difficulty in error analysis and in the numerical methods is the low regularity of solution resulted from nonsmooth interfaces, which is a well-known natural phenomenon called tip-geometry effect in many fields. When the interface is Lipschitz continuous and solution is C^1 or H^2 continuous, the best known result in the literature is of 1st – 1.5th order convergence in solution and 0.7 order of convergence in the gradient [21]. It is demonstrated that the piecewise constant WG-FEM achieves at least an order of 1.75 convergence in the solution and an order of 1 convergence in the gradient. A numerical study of higher order WG methods for solving interface problems with low solution regularities and sharp edges shall be conducted for a better understanding of the WG-FEM.

References

[1] I. Babuška, The finite element method for elliptic equations with discontinuous coefficients, Computing 5 (1970) 207–213.
[2] J.T. Beale, A.T. Layton, On the accuracy of finite difference methods for elliptic problems with interfaces, Commun. Appl. Math. Comput. Sci. 1 (2006) 91–119.
[3] J. Bedrossian, J.H. von Brecht, S.W. Zhu, E. Sifakis, J.M. Teran, A finite element method for interface problems in domains with smooth boundaries and interfaces, J. Comput. Phys. 229 (2010) 6405–6426.
[4] J. Bramble, J. King, A finite element method for interface problems in domains with smooth boundaries and interfaces, Adv. Comput. Math. 6 (1996) 109–138.
[5] E. Burman, P. Hansbo, Interior-penalty-stabilized Lagrange multiplier methods for the finite-element solution of elliptic interface problems, SIAM J. Numer. Anal. 30 (2010) 870–885.
[6] Z. Cai, X. Ye, S. Zhang, Discontinuous Galerkin finite element methods for interface problems: a priori and a posteriori error estimations, SIAM J. Numer. Anal. 49 (2011) 1761–1787.
[7] D. Chen, Z. Chen, C. Chen, W.H. Geng, G.W. Wei, MIBPB: a software package for electrostatic analysis, J. Comput. Chem. 32 (2011) 657–670.
[8] T. Chen, J. Strain, Piecewise-polynomial discretization and Krylov-accelerated multigrid for elliptic interface problems, J. Comput. Phys. 16 (2008) 7503–7542.
[9] M. Dryjaa, J. Galvisb, M. Sarkisb, BDDC methods for discontinuous Galerkin discretization of elliptic problems, J. Complexity 23 (2007) 715–739.
[10] R.E. Ewing, Z.L. Li, T. Lin, Y.P. Lin, The immersed finite volume element methods for the elliptic interface problems, Math. Comput. Simul. 50 (1999) 63–76.
[11] R.P. Fedkiw, T. Aslam, B. Merriman, S. Osher, A non-oscillatory Eulerian approach to interfaces in multimaterial flows (the ghost fluid method), J. Comput. Phys. 152 (1999) 457–492.
[12] W.H. Geng, S.N. Yu, G.W. Wei, Treatment of charge singularities in implicit solvent models, J. Chem. Phys. 127 (2007) 114106.

[13] R. Glowinski, T.-W. Pan, J. Periaux, A fictitious domain method for Dirichlet problem and applications, Comput. Methods Appl. Mech. Eng. 111 (1994) 283–303.
[14] G.R. Hadley, High-accuracy finite-difference equations for dielectric waveguide analysis I: uniform regions and dielectric interfaces, J. Lightwave Technol. 20 (2002) 1210–1218.
[15] A. Hansbo, P. Hansbo, An unfitted finite element method, Comput. Methods Appl. Mech. Eng. 191 (2002) 5537–5552.
[16] I. Harari, J. Dolbow, Analysis of an efficient finite element method for embedded interface problems, Comput. Math. 46 (2010) 205–211.
[17] X. He, T. Lin, Y. Lin, Interior penalty bilinear IFE discontinuous Galerkin methods for elliptic equations with discontinuous coefficient, J. Syst. Sci. Complexity 23 (2010) 467–483.
[18] J.S. Hesthaven, High-order accurate methods in time-domain computational electromagnetics. a review, Adv. Imag. Electron Phys. 127 (2003) 59–123.
[19] R. Hiptmair, J. Li, J. Zou, Convergence analysis of finite element methods for H(div;Omega)-elliptic interface problems, J. Numer. Math. 18 (2010) 187–218.
[20] T.P. Horikis, W.L. Kath, Modal analysis of circular Bragg fibers with arbitrary index profiles, Opt. Lett. 31 (2006) 3417–3419.
[21] S.M. Hou, W. Wang, L.Q. Wang, Numerical method for solving matrix coefficient elliptic equation with sharp-edged interfaces, J. Comput. Phys. 229 (2010) 7162–7179.
[22] T.Y. Hou, Z.L. Li, S. Osher, H.K. Zhao, A hybrid method for moving interface problems with application to the Heleshaw flow, J. Comput. Phys. 134 (2) (1997) 236–252.
[23] A.T. Layton, Using integral equations and the immersed interface method to solve immersed boundary problems with stiff forces, Comput. Fluids 38 (2009) 266–272.
[24] R.J. LeVeque, Z.L. Li, The immersed interface method for elliptic equations with discontinuous coefficients and singular sources, SIAM J. Numer. Anal. 31 (1994) 1019–1044.
[25] A. Mayo, The fast solution of Poisson's and the biharmonic equations on irregular regions, SIAM J. Numer. Anal. 21 (1984) 285–299.
[26] L. Mu, J. Wang, Y. Wang, X. Ye, A computational study of the weak Galerkin method for the second-order elliptic equations, Numer. Algorithm (2012). http://dx.doi.org/10.1007/s11075-012-9651-1.
[27] L. Mu, J. Wang, X. Ye, and S. Zhao. A numerical study on the weak Galerkin method for the Helmholtz equation with large wave numbers, 2012. Available at: <arXiv:1111.0671v1>.
[28] M. Oevermann, R. Klein, A Cartesian grid finite volume method for elliptic equations with variable coefficients and embedded interfaces, J. Comput. Phys. 219 (2006) 749–769.
[29] C.S. Peskin, D.M. McQueen, A 3-dimensional computational method for blood-flow in the heart. 1. Immersed elastic fibers in a viscous incompressible fluid, J. Comput. Phys. 81 (1989) 372–405.
[30] C.S. Peskin, Numerical analysis of blood flow in the heart, J. Comput. Phys. 25 (3) (1977) 220–252.
[31] I. Ramiere, Convergence analysis of the q_1-finite element method for elliptic problems with non-boundary-fitted meshes, Int. J. Numer. Methods Eng. 75 (2008) 1007–1052.
[32] P.A. Raviart, J.M. Thomas, A mixed finite element method for 2-nd order elliptic problems, in: A. Dold, B. Eckmann (Eds.), Mathematical Aspects of Finite Element Methods, Lecture Notes in Mathematics Series, vol. 606, Springer, Berlin, 1977, pp. 92–315.
[33] D.A. Wang, R. Li, N.N. Yan, An edge-based anisotropic mesh refinement algorithm and its application to interface problems, Commun. Comput. Phys. 8 (2010) 511–540.
[34] J. Wang, X. Ye, A weak Galerkin finite element method for second-order elliptic problems, J. Comput. Appl. Mech. 241 (2013) 103–115.
[35] X.S. Wang, L.T. Zhang, L.W. Kam, On computational issues of immersed finite element methods, J. Comput. Phys. 228 (2009) 2535–2551.
[36] K.N. Xia, M. Zhan, G.-W. Wei, The matched interface and boundary (MIB) method for multi-domain elliptic interface problems, J. Comput. Phys. 230 (2011) 8231–8258.
[37] S.N. Yu, G.W. Wei, Three-dimensional matched interface and boundary (MIB) method for treating geometric singularities, J. Comput. Phys. 227 (2007) 602–632.
[38] S.N. Yu, Y. Zhou, G.W. Wei, Matched interface and boundary (MIB) method for elliptic problems with sharp-edged interfaces, J. Comput. Phys. 224 (2) (2007) 729–756.
[39] S.N. Yu, W.H. Geng, G.W. Wei, Treatment of geometric singularities in implicit solvent models, J. Chem. Phys. 126 (2007) 244108.
[40] S. Zhao, High order matched interface and boundary methods for the Helmholtz equation in media with arbitrarily curved interfaces, J. Comput. Phys. 229 (2010) 3155–3170.
[41] S. Zhao, G.W. Wei, High-order FDTD methods via derivative matching for Maxwell's equations with material interfaces, J. Comput. Phys. 200 (1) (2004) 60–103.
[42] Y.C. Zhou, G.W. Wei, On the fictitious-domain and interpolation formulations of the matched interface and boundary (MIB) method, J. Comput. Phys. 219 (1) (2006) 228–246.
[43] Y.C. Zhou, S. Zhao, M. Feig, G.W. Wei, High order matched interface and boundary method for elliptic equations with discontinuous coefficients and singular sources, J. Comput. Phys. 213 (1) (2006) 1–30.
[44] L. Mu, J. Wang, and X. Ye, A Weak Galerkin Finite Element Method with Polynomial Reduction, 2013. Available at: <arxiv:1304:6481>.
[45] J. Wang and X. Ye, A weak Galerkin mixed finite element method for second-order elliptic problems, 2012. Available at: <arXiv:1202.3655>.